Q. J. R. Meteorol. Soc. (2000), **126**, pp. 1–999

The influence of the 1997–1999 ENSO on extratropical baroclinic life cycles over the Eastern North Pacific

By M. A. SHAPIRO[1*], H. WERNLI[2], N. A. BOND[3], and R. LANGLAND[4]

[1]*NOAA, Environmental Technology Laboratory, Boulder, Colorado, U.S.A.*

[2]*Institute for Atmospheric Science, ETH, Zurich, Switzerland*

[3]*Joint Institute for the Study of the Atmosphere and Ocean, University of Washington, Seattle, U.S.A.*

[4]*Naval Research Laboratory, Monterey, California, U.S.A.*

Summary

The El Niño-Southern Oscillation (ENSO) strongly influences the interannual and seasonal atmospheric circulation over the North Pacific. The present study shows that the meridional displacement of the time-mean upper-level jet associated with ENSO modulates the time-mean barotropic (meridional) wind shear over the central and eastern North Pacific storm track. Earlier theoretical and observational studies established the influence of barotropic wind shear on the life cycles of extratropical cyclones and their upper-level potential vorticity (PV) waves. The present study suggests that differences in the time-mean flow associated with the 1997–1999 ENSO cycle had a similar impact on tropopause PV structure, meridional eddy fluxes of momentum and temperature, and predictability.

Keywords: El Niño Baroclinic waves Potential vorticity

1. Introduction and Background

The North Pacific wintertime atmospheric circulation is known to respond to the variations in the tropical Pacific atmosphere-ocean climate system, especially to ENSO. As reviewed by Trenberth *et al.* (1998), past research on the impacts of ENSO on the extratropics has focused mostly on seasonal mean phenomena, such as geopotential height

* Corresponding author: Dr. M. A. Shapiro, NCAR, P.O. Box 3000, Boulder, CO 80307 U.S.A; mshapiro@ncar.ucar.edu

anomalies, shifts in mid-latitude storm tracks, and their impacts on precipitation and surface temperature. The ability to anticipate these impacts provides much, if not most, of our present skill in seasonal weather prediction over many parts of the world (e.g., Barnston and Smith 1996). By comparison, the influence of ENSO on the life cycles of individual extratropical baroclinic disturbances and their attendant PV structures, fronts, and precipitation has received less attention. An exception is provided by Barsugli *et al.* (1999) in a study of the effects of the 1997–98 El Niño on three severe weather events. We begin by reviewing the impact of ENSO on the extratropical seasonal circulation, followed by a discussion of earlier studies on the influence of variations in planetary-scale flows on baroclinic life cycles.

(*a*) *ENSO Signatures*

The impact of ENSO on the time-mean extratropical atmospheric circulation is reasonably well understood. Anomalies in tropical deep convection associated with ENSO modulate the Hadley circulation, with consequent effects on the strength and location of the subtropical jet stream (Bjerknes 1969). Modulations of the local meridional (Hadley) circulation are also manifested as anomalies in upper-tropospheric subtropical divergence. This divergence, in the presence of the background vorticity gradient, represents a source for Rossby wave propagation into higher latitudes (e.g., Sardeshmukh and Hoskins 1988). The linkages between ENSO and the wintertime North Pacific and North America circulation are quite strong and account for the substantial correlations found between ENSO and preferred modes of large-scale extratropical variability, such as the Pacific-North American (PNA) pattern (Horel and Wallace 1981). One of the most robust signals of ENSO is its modulation of the intensity and position of the seasonal time-mean upper-level jet stream over the Eastern North Pacific. This variation in the time-mean flow occurs north of the region of maximum amplitude in the ENSO tropical precipitation

signal. This flow characteristic is illustrated in the 250-mb wind velocity analysis for the most recent ENSO (Fig. 1). The salient feature in Fig. 1 is the strengthening and southward displacement of the jet east of the date line during the El Niño of 1998 (Fig. 1a) and its weakening and northward displacement during the La Niña of 1999 (Fig. 1b), as compared with the climatological mean (not shown). For future reference, we draw attention to these differences in time-mean meridional shear within the latitudinal belt (30–50°N) that coincides with the preferred zone for transient synoptic-scale eddies, i.e., the storm track. The 250-mb time-mean flows for El Niño, 1998 and La Niña, 1999 were representative of composites based on the last 7 El Niños and 6 La Niñas (not shown). We consider the influence of these variations in meridional shear on baroclinic life cycles in section 2.

(*b*) *Planetary-scale Influences*

The influence of planetary-scale meridional shear on the life cycles of extratropical cyclones was first shown through numerical simulations of idealized atmospheres (e.g., Hoskins 1990; Davies *et al.* 1991; Thorncroft *et al.* 1993). These studies revealed that the evolution of idealized cyclones (anticyclones) and their associated fronts, upper-level PV, and eddy fluxes of heat and momentum is sensitive to a small meridional barotropic wind shear component superimposed upon an otherwise symmetric zonal basic state flow. Cyclones evolving in a non-sheared environment were referred to as Life Cycle 1 (LC1); those evolving in a cyclonically sheared environment were referred to as Life Cycle 2 (LC2). Shapiro *et al.* (1999) extended this dynamical perspective to the analysis of simulations of actual baroclinic life cycles. The observed LC1 baroclinic developments evolved beneath the core of the upper jet, while LC2 developments occurred on the cyclonic-shear side of the upper jet. Simmons (1999) presented representative examples of the upper-level PV wave structure associated with the two contrasting life cycles

(Fig. 2). The typical LC2 PV structure (Fig. 2a) is characterized by forward (cyclonic) PV roll up, whereas rearward (anticyclonic) wave breaking and filamentation are evident in the LC1 example (Fig. 2b). We have previously noted the substantial differences in the environmental time-mean upper-level flow and its associated meridional shear over the eastern Pacific during different phases of ENSO (Fig. 1). Might we therefore anticipate ENSO modulation of the character of baroclinic life cycles over the eastern North Pacific? It is this question that is addressed in this study.

2. Time-Mean Flow Influences on Baroclinic Life Cycles during the 1997–1999 ENSO

One of the strongest El Niños on record occurred during 1997–1998. In anticipation of potentially extreme El Niño related storms and associated flooding along the western U.S. coastal zone during the winter of 1998, the National Oceanic and Atmospheric Administration (NOAA), Office of Naval Research, and U.S. Air Force Reserve 53rd Weather Reconnaissance Wing provided support for the North Pacific Experiment (NORPEX, Langland *et al.* 1999). NORPEX deployed targeted dropwindsondes over the eastern North Pacific in order to improve 1–3 day forecasts and warnings for landfalling storms. These targeted observations were continued during the 1999 La Niña under the NOAA Environmental Modeling Center's Winter Storm Reconnaissance Program (WSRP) (Toth *et al.* 2000). It was the authors' involvement in these targeted observing programs that stimulated their present interest in investigating ENSO modulation of individual extratropical weather systems.

(*a*) *Jet-Stream Time-Mean Meridional Structure*

We now present time-mean meridional cross-sections across the Eastern North Pacific upper-level jet stream for January–February 1998 and 1999. Figure 3 shows cross

sections of zonal wind, potential temperature, and PV tropopause at 130°W. This longitude is the typical location of the maximum ENSO-related anomalies in the jet. The key features during the 1998 El Niño (Fig. 3a) were the ∼50 m s^{-1} 200-mb jet core at 30°N and the zone of cyclonic meridional shear between 35–55°N that extends from the stratosphere to the ocean. During the 1999 La Niña (Fig. 3b), there was a weaker and more symmetric ∼30 m s^{-1} 250-mb jet core at 45°N, with minimal meridional shear in the vicinity of 45°N. A comparison between the two cross-sections reveals the following aspects related to ENSO: i) latitudinal displacements of the jet over the eastern Pacific and differing meridional shear in the latitudes of the baroclinic waves; ii) increased middle- to upper-tropospheric baroclinity in the subtropics during El Niño in response to enhanced deep tropical convection; iii) relatively cooler tropospheric temperatures at northern latitudes during La Niña; and iv) a steeper slope of the potential vorticity tropopause in the vicinity of the jet core during El Niño. It should also be recognized that these aspects are not unique to ENSO. In other words, variability intrinsic to the extratropical atmosphere can bring about similar flow configurations, in the absence of ENSO-related tropical forcing.

The El Niño-related mean flow anomalies are modulated by intraseasonal fluctuations in tropical deep convection. During the El Niño of 1998, particularly intense convection occurred in the eastern tropical Pacific between 26 January and 7 February in coincidence with an especially strong subtropical jet in the eastern Pacific.

(*b*) *PV Wave Characteristics (LC1 vs. LC2) during ENSO*

Representative examples of upper-level PV waves from the 1997–1999 ENSO are shown in Fig. 4. The example from El Niño (Fig. 4a) is a typical forward-breaking PV wave during a LC2 life cycle, as revealed in the color-shaded 320-K PV. In contrast, the example from La Niña (Fig. 4b) represents a prominent LC1 rearward-breaking PV wave

on both the 320- and 340-K surfaces, including a narrowing filament of stratospheric PV extending into the subtropics. These two examples mirror both the theoretically idealized (e.g., Thorncroft *et al.* 1993) and observed (e.g., Fig. 2) life cycles. It is recognized that different meridional tilts of the upper-level PV ridge/trough axes (e.g., Figs. 2 and 4) are associated with significantly different meridional momentum fluxes. The PV fields shown in Fig. 4 portray well-defined, but by no means atypical, examples of the LC2 (LC1) PV waves that occurred preferentially during the period of El Niño (La Niña). As a measure for this preference for a given type of baroclinic life cycle, we used 1200 UTC European Center for Medium-Range Weather Forecasting (ECMWF) analyses to tabulate the number of events during the period 16 January through 28 February in 1998 and 1999, during which the eastern North Pacific (from the dateline to 120°W) was characterized by LC1 and LC2 PV distributions. The selection of LC1 versus LC2 events was determined from the sense of the PV wave breaking; anticylonic versus cyclonic, respectively. LC1 days were identified as those with PV maxima oriented SW to NE that extended well into the subtropics. LC2 days were those with zero to negative tilts in PV maxima. Another criterion of identifying LC1 versus LC2 characteristics was the relative amplitude and poleward extension of the negative PV anomalies flanking the PV maxima, i.e., greater negative anomalies to the west (east) for LC1 (LC2). The results for the 1998 El Niño were 26 days of LC2 PV signatures in association with 16 individual LC2 events, and 4 days with LC1 signatures in association with 3 individual LC1 events. During the 1999 La Niña, on the other hand, there were only 3 days and 2 events with LC2 PV signatures, while there were 27 days and 7 events with LC1 signatures.

(*c*) *Meridional Eddy Flux Diagnostics*

Thorncroft *et al.* (1993) showed significant differences in the poleward momentum and heat fluxes between idealized LC1 and LC2 experiments. Previous studies (notably,

Trenberth and Hurrel 1994) have clearly shown the effects of differences in the time-mean flow over the North Pacific on the momentum and heat fluxes associated with eddy-mean flow interactions. The importance of these interactions during a period of anomalous upper-level zonal flow over the east Pacific was shown by Mo *et al.* (1995). The preference for LC2 and LC1 life cycles during January–February 1998 and 1999, respectively (Fig. 4), led us to explore the possible link between their prevalence and the differences in eddy-mean flow interactions during the 1997–1999 ENSO. For this purpose, we use the framework of "localized" Eliassen-Palm (EP) fluxes (Trenberth 1986), which pertain to the effects of transient eddies on the local zonal flow. The two principal contributions to these fluxes tend to be the meridional fluxes of zonal momentum aloft and of temperature in the low to middle troposphere. These contributions have been band-pass filtered (using the recursive Murakami technique (Murakami 1979), with a band from 2.5 to 8 days) and are compared for January–February 1998 and 1999 in Fig. 5. The 1998 El Niño featured poleward (positive) eddy momentum fluxes at 250 mb (Fig. 5a) that were distributed in a narrow (20°) belt along the time-mean jet axis (Fig. 1a), with maximum amplitude at 160°W. In contrast, during the 1999 La Niña eddy momentum fluxes (Fig. 5b) bifurcated at 35°N, 170°W with one branch following the northward displaced jet over the Eastern Pacific and the other extending well into subtropical latitudes, in the region of preferred anticyclonic wave breaking (Fig. 4b). There were also significant differences in low-level poleward eddy temperature fluxes in the two periods, the most notable being larger values over the Eastern Pacific during La Niña (Fig. 5b). These larger amplitude temperature fluxes were in the region of enhanced surface anticyclones (not shown) associated with LC1 upper-level anticyclonic wave breaking. The differences between the two years extend across the U.S. and Northern Mexico.

Latitude-height cross sections for the longitude band 140–160°W provide a complementary perspective on the characteristics of the meridional fluxes of momentum and heat due to the transient eddies (Fig. 6). A comparison between the cross-sections for El Niño of 1998 and La Niña of 1999 (Fig. 6a and b, respectively) reveals the following differences: i) the meridional momentum flux featured a single upper-level maximum near 30°N in 1998 (Fig. 6a) versus two maxima between 25° and 40°N in 1999 (Fig. 6b), ii) the meridional heat flux was weaker and decreased more rapidly with height during 1998 when LC2 predominated, than during 1999 when LC1 predominated. These results indicate a significantly different forcing of the time-mean flow by the eddies in the two phases of this ENSO.

We suggest that LC1 PV life cycles over the eastern North Pacific are often associated with Rossby wave propogation from the extratropical to tropical latitudes described by Kiladis (1998) and Matthews and Kiladis (1999), among others. This energy dispersion process typically begins with high-latitude (∼50°N) cyclogenesis east of Japan followed by downstream LC1 PV wave breaking in subtropical latitudes (as in Fig. 4b), culminating with enhanced convection at the ITCZ. Matthews and Kiladis (1999) reported that high-to-low latitude Rossby wave propagation is suppressed during the El Niño phase of ENSOs. They found no cross-equatorial propagation of wave activity during the 1997–98 El Niño, which is consistent with our finding of very few (and weak) LC1 events.

(*d*) *ENSO Impact on Short-Range Predictability*

Another point of interest is the effect of ENSO on the predictability of atmospheric flows. Here we compare the error of 72-h forecasts during January and February of 1998 and 1999 made by the Navy Operational Global Atmospheric Prediction System (NOGAPS) using identical versions of the model and data assimilation system. The mean error of the forecasts verifying over western North America was 21% larger during 1999

than during 1998 (Fig. 7). A Kolmogorov-Smirnov test indicates that the forecast error was greater in 1999 than in 1998 with a confidence level of 93.9%. We have also considered just the 13-day periods between 26 January and 7 February of both years, when the LC2 and LC1 related flow anomalies were at peak intensity. The forecast errors were 55% larger during 1999, when LC1 predominated. This difference has a confidence level of 91.3%. This 13-day period in 1999 was marked by a strong ridging over the mid-Pacific with troughing along the west coast of North America. This suggests that predictability may be lower when strong anti-cyclonic wave breaking (a process not restricted to times of La Niña) occurs upstream of a forecast verification region. Finally, it is recognized that additional factors, such as the amplitude and area of initial analysis error sensitivities, impact on predictability.

3. Future Considerations

This short contribution strongly suggests that anomalies in the time-mean environmental flow associated with El Niño and La Niña lead to preferential baroclinic life cycles over the Eastern North Pacific that closely mimic the idealized LC2 and LC1 paradigms, respectively. We recognize that our results are based on only two years and are more suggestive than definitive. An obvious next step is to extend the present diagnostics and predictability studies to additional ENSO events. We suggest that future work could address the following topics: i) the influence of LC1/LC2 wave-mean flow interactions on seasonal-mean ENSO circulation anomalies (e.g., Kok and Opsteegh 1985), ii) ENSO modulation of downstream (upstream) energy dispersion (e.g., Wernli *et al.* 1999), iii) the ability of climate models currently used for seasonal and interannual predictions to resolve the characteristics of LC1/LC2 life cycles, iv) the possible modulation by ENSO of the location and amplitude of sensitive regions within which initial analysis errors

strongly impact the 1–10 day predictability of weather events. If the latter effects are significant and systematic, ENSO forecasts could be used in the design of observing systems and strategies for improving 1–6 day numerical weather prediction over and downstream of the relatively data-sparse North Pacific Ocean.

Acknowledgements

The authors thank David N. Bresch for providing the band-pass filtering routine. We acknowledge the use of the NCEP/NCAR Reanalysis and the tools provided by NOAA's Climate Diagnostic Center in the production of Fig. 1, and analyses from ECMWF in the production of Figs. 3–6. We acknowledge and thank the U.S. Office of Naval Research (N0001499F0068) support of this collaborative research. Contribution 2144 from NOAA/PMEL. Contribution 729 from JISAO.

References

Barnston, A. G., and T. M. Smith 1996 Specification and prediction of global surface temperature and precipitation from global SST using CCA. *J. Clim.* **9,** 2660–2697

Barsugli, J. J., J. S. Whitaker, A. F. Loughe, P. D. Sardeshmukh, and Z. Toth 1999 The effect of the 1997/98 El Niño on individual large-scale weather events. *Bull. Amer. Meteorol. Soc.* **80,** 1399–1411

Bjerknes, J. 1969 Atmospheric teleconnections from the equatorial Pacific. *Mon. Wea. Rev.* **97,** 163–172

Davies, H. C., C. Schär, and H. Wernli 1991 The palette of fronts and cyclones within a baroclinic wave development. *J. Atmos. Sci.* **48,** 1666–1689

Horel, J. D., and J. M. Wallace 1981 Planetary scale atmospheric phenomena associated with the Southern Oscillation. *Mon. Wea. Rev.* **109,** 813–829

Hoskins, B. J. 1990 Theory of extratropical cyclones. Extratropical Cyclones, Palmén Memorial Volume, C. W. Newton and E. O. Holopainen, Eds., *Am. Meteorol. Soc.* 63–80

Kiladis, G. N. 1998 Observations of Rossby waves linked to convection over the eastern tropical Pacific. *J. Atmos. Sci.* **55,** 321–339

Kok, C. J., and J. D. Opsteegh 1985 On the possible causes of anomalies in seasonal mean circulation pattern during the 1982–83 El Niño event. *J. Atmos. Sci.* **42,** 677–694

Langland, R. H, and Collaborators 1999 The North Pacific Experiment (NORPEX-98): Targeted observations for improved North American weather forecasts. *Bull. Am. Meteorol. Soc.* **80,** 1363–1384

Matthews, A. J., and G. N. Kiladis 1999 Interactions between ENSO, transient circulation, and tropical convection over the Pacific. *J. Clim.* **12,** 3062-3086

Mo, K. C., J. Nogues-Paegle, and J. Paegle 1995 Physical mechanisms of the 1993 summer floods. *J. Atmos. Sci.* **52,** 879–895

Murakami, M. 1979 Large-scale aspects of deep convective activity over the GATE area. *Mon. Wea. Rev.* **107,** 994–1013

Sardeshmukh, P. D., and B. J. Hoskins 1988 The generation of global rotational flow by steady idealized tropical divergence. *J. Atmos. Sci.* **45,** 1228–1251

Shapiro, M., and Collaborators	1999	A planetary-scale to mesoscale perspective of the life cycles of extratropical cyclones. *The life cycles of extratropical cyclones,* M. A. Shapiro and S. Gronås, Eds., *Am. Meteorol. Soc.* 139–186
Simmons, A.	1999	Numerical simulations of cyclone life cycles. *The life cycles of extratropical cyclones,* M. A. Shapiro and S. Gronås, Eds., *Am. Meteorol. Soc.* 123–137
Thorncroft, C. D., B. J. Hoskins, and M. E. McIntyre	1993	Two paradigms of baroclinic-wave life cycle behavior. *Quart. J. Roy. Meteorol. Soc.* **119,** 17–55
Toth, Z., I. Szunyogh, S. Majumdar, R. Morss, B. Etherton, C. Bishop, and S. Lord	2000	Targeted observations at NCEP: Toward an operational implementation. Fourth Symposium on Integrated Observing Systems, Jan. 10–14, 2000, Long Beach, CA, Amer. Meteorol. Soc., 186–193
Trenberth, K. E.	1986	An assessment of the impact of transient eddies on the zonal flow during a blocking episode using localized Eliassen-Palm flux diagnostics. *J. Atmos. Sci.* **43,** 2070–2087
Trenberth, K. E., and J. W. Hurrell	1994	Decadal atmosphere-ocean variations in the Pacific. *Clim. Dynamics* **9,** 303–319
Trenberth, K. E., G. W. Branstator, D. Karoly, A. Kumar, N.-C. Lau, and C. Ropelewski	1998	Progress during TOGA in understanding and modeling global teleconnections associated with tropical sea surface temperatures. *J. Geophys. Res.* **103,** 14,291–14,324

Wernli, H., M. A. Shapiro, and J. Schmidli 1999 Upstream development in idealized baroclinic wave experiments. *Tellus* **51A,** 574–587.

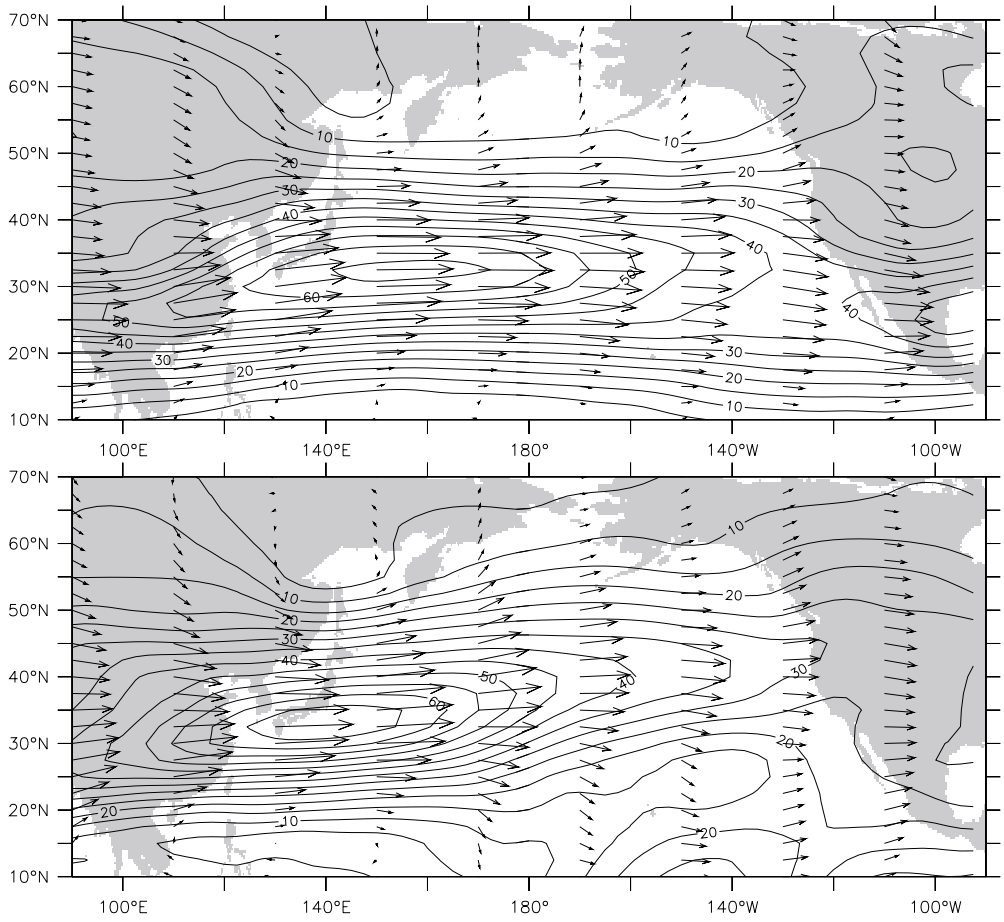

Figure 1. January–March time-mean 250-mb wind speed (m s^{-1}, lines) and vectors (arrows): (top) for the El Niño year 1998; (bottom) for the La Niña year 1999 (NOAA-CIRES/Climate Diagnostic Center).

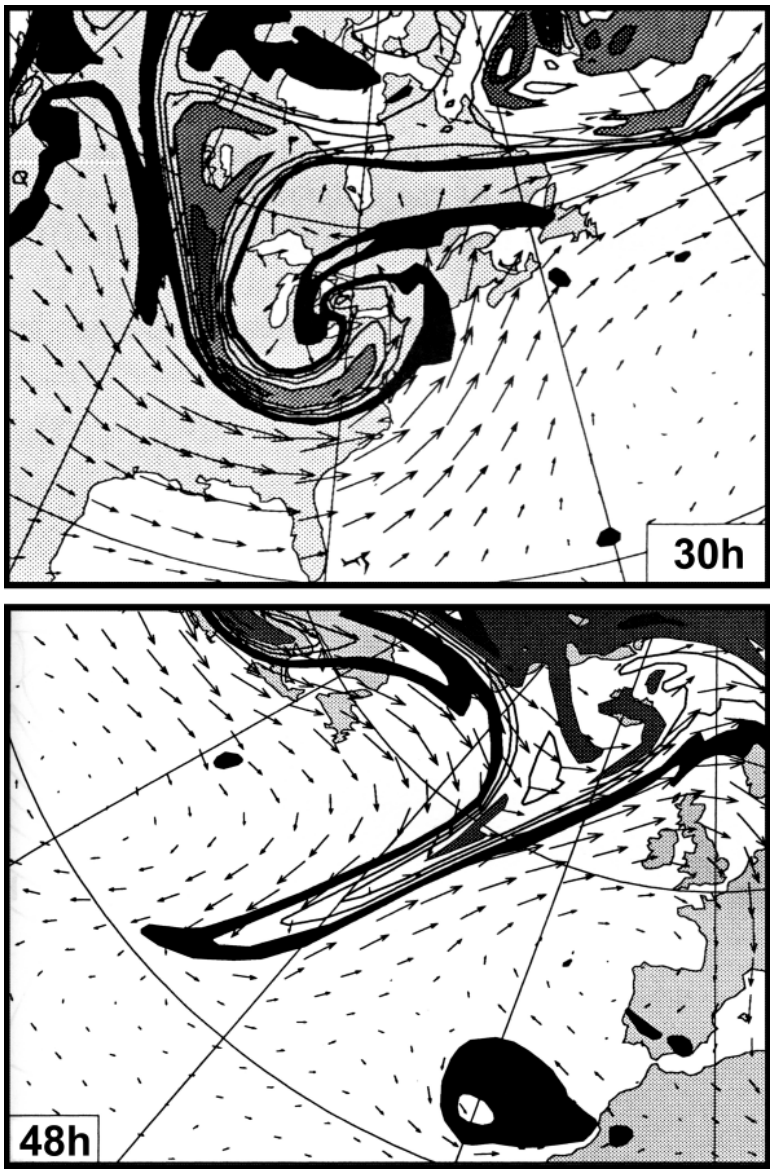

Figure 2. Potential vorticity (shaded at 1 PVU intervals, black; 1-2 PVU) and wind vectors: (top) 1800 UTC 26 January 1978 at 310 K; (bottom) 1200 UTC 29 Jan 1994 at 315 K isentropic surface (Simmons 1999).

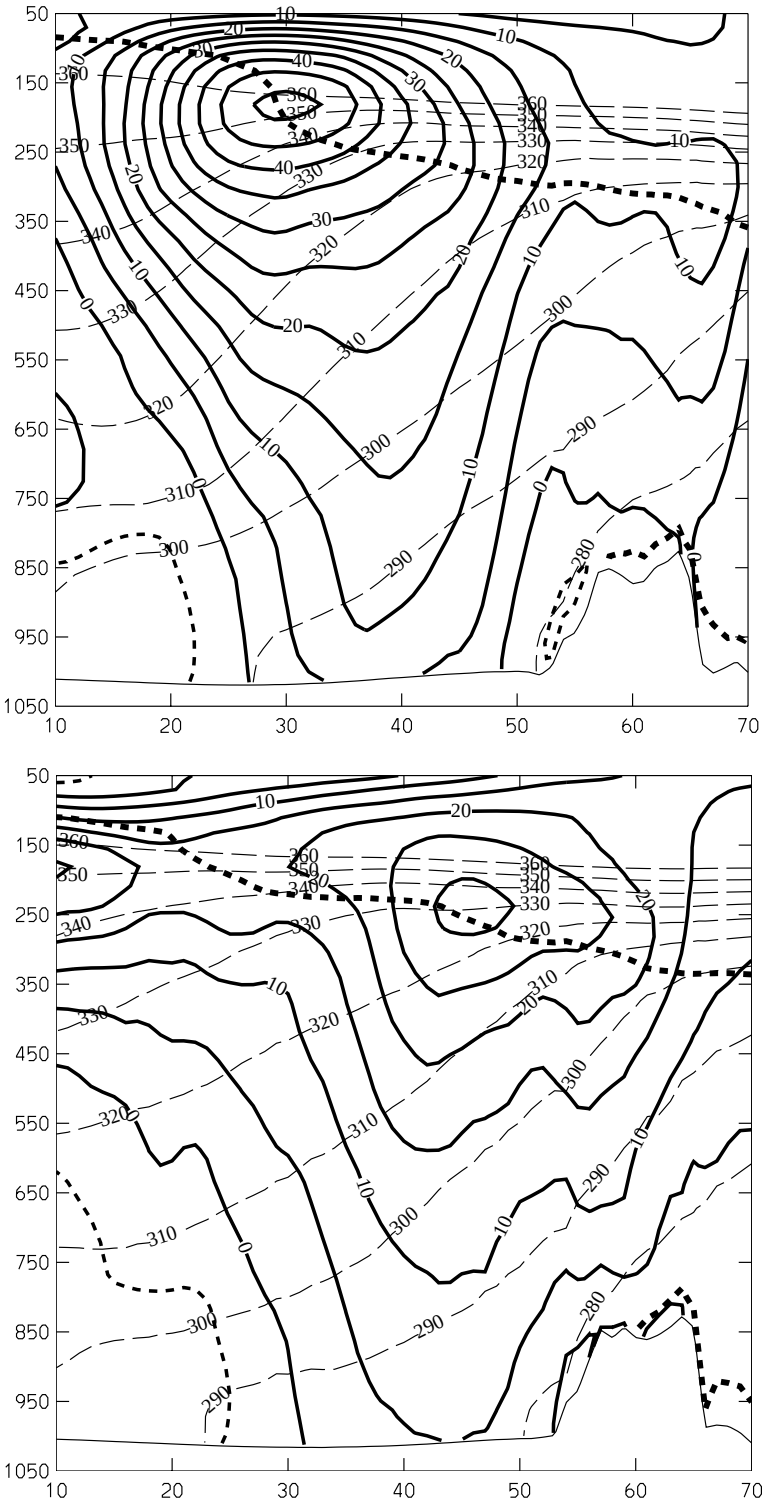

Figure 3. January–February time-mean meridional cross sections at 130°W for (top) 1998; (bottom) 1999: zonal wind (5 m s^{-1} intervals, solid lines); potential temperature (10-K intervals between 280–360 K, long dashed lines); 2-PVU tropopause, short-dashed line (ECMWF analyses).

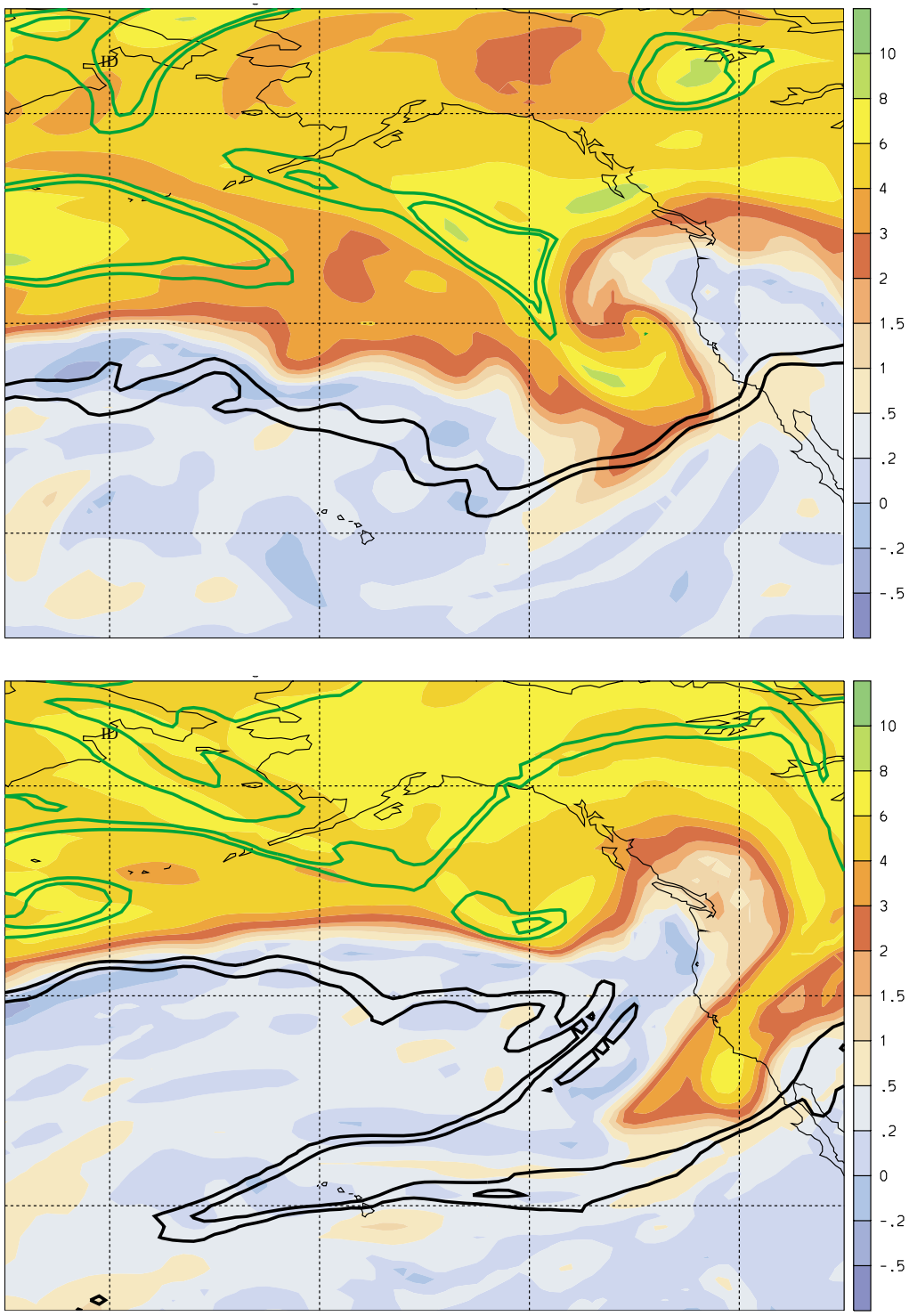

Figure 4. Potential vorticity at three isentropic levels for (top) 1200 UTC 6 February 1998 (El Niño); (bottom) 1200 UTC 5 February 1999 (La Niña). 300-K PV (green lines, 2 and 3 PVUs); 320-K PV (color shading, PVU, as in color bar); 340-K PV (black lines, 2 and 3 PVUs) (ECMWF analyses).

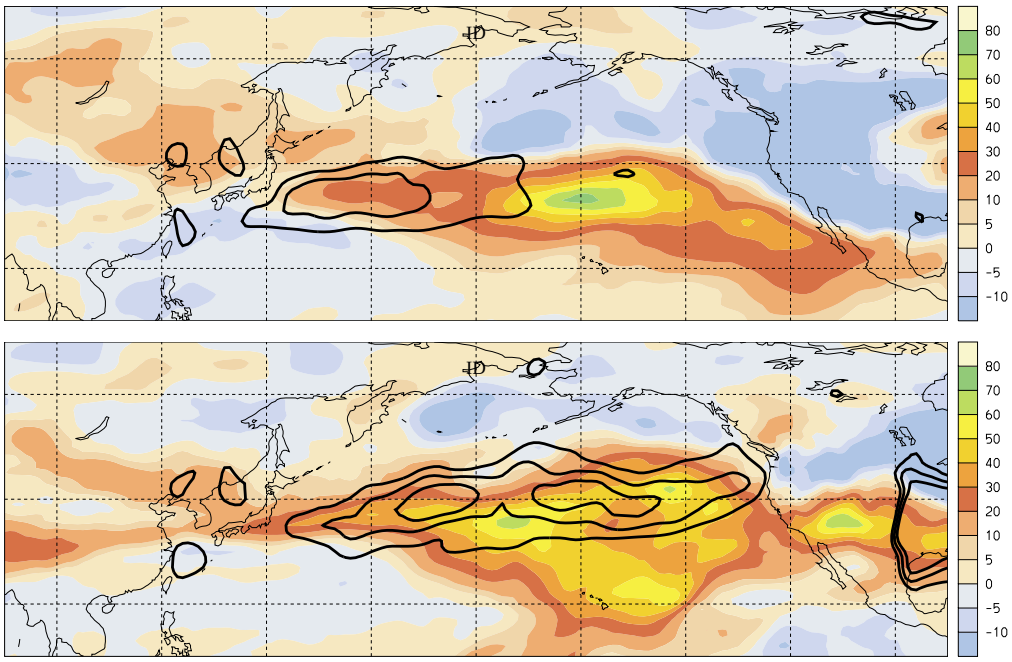

Figure 5. January–February time-mean, band-pass filtered meridional eddy fluxes of 250-mb momentum and 925-mb temperature: (top) 1998; (bottom) 1999. Momentum flux (m^2 s^{-2}, as in color bar). Temperature flux; isolines at 6, 8, and 10 K m s^{-1} (ECMWF analyses).

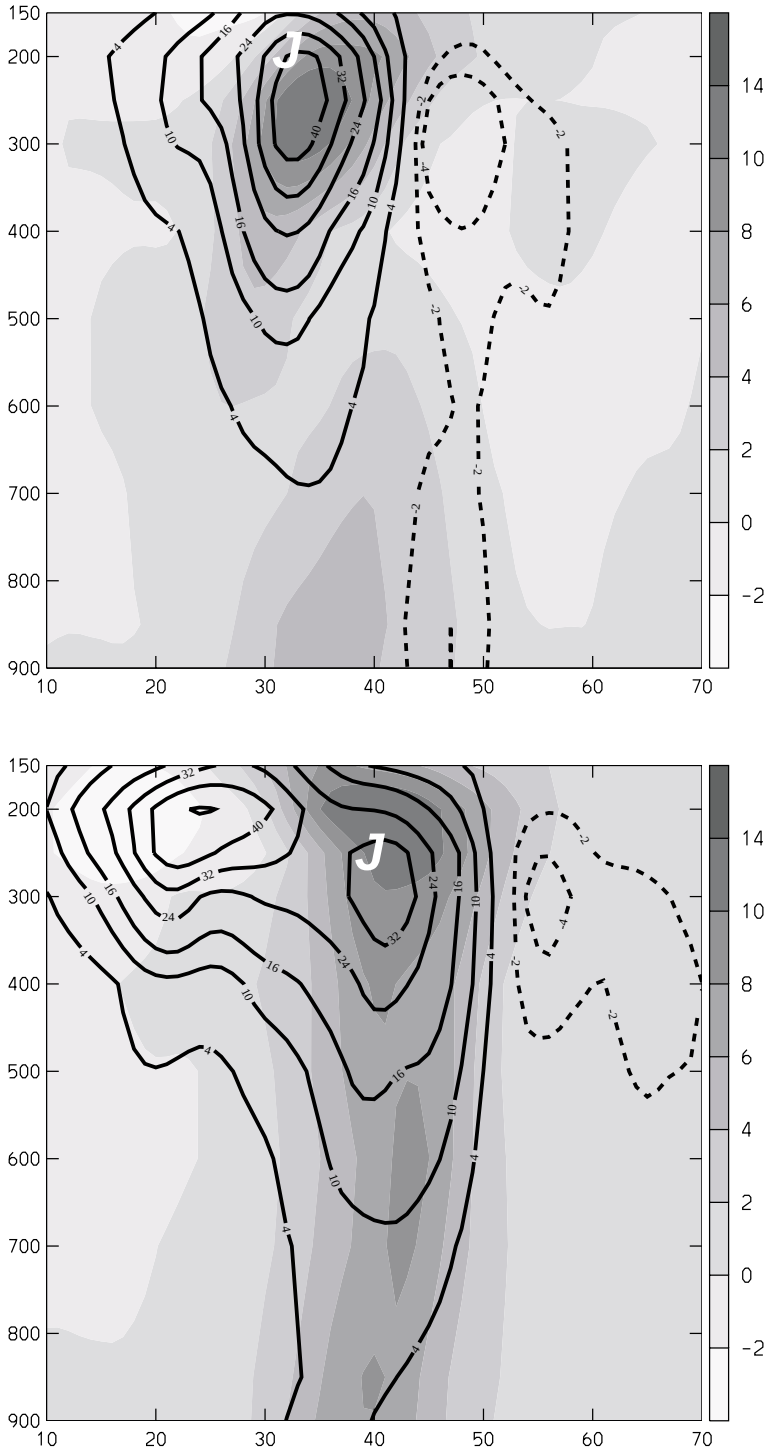

Figure 6. Zonally averaged (between 140 and 160°W) January–February time-mean, band-pass filtered meridional eddy fluxes of temperature (K m s^{-1}, grey shading) and momentum (isolines at irregular intervals from –8 to 50 m^2 s^{-2}) for 1998 (panel a) and 1999 (panel b). All fields are derived from ECMWF analyses.

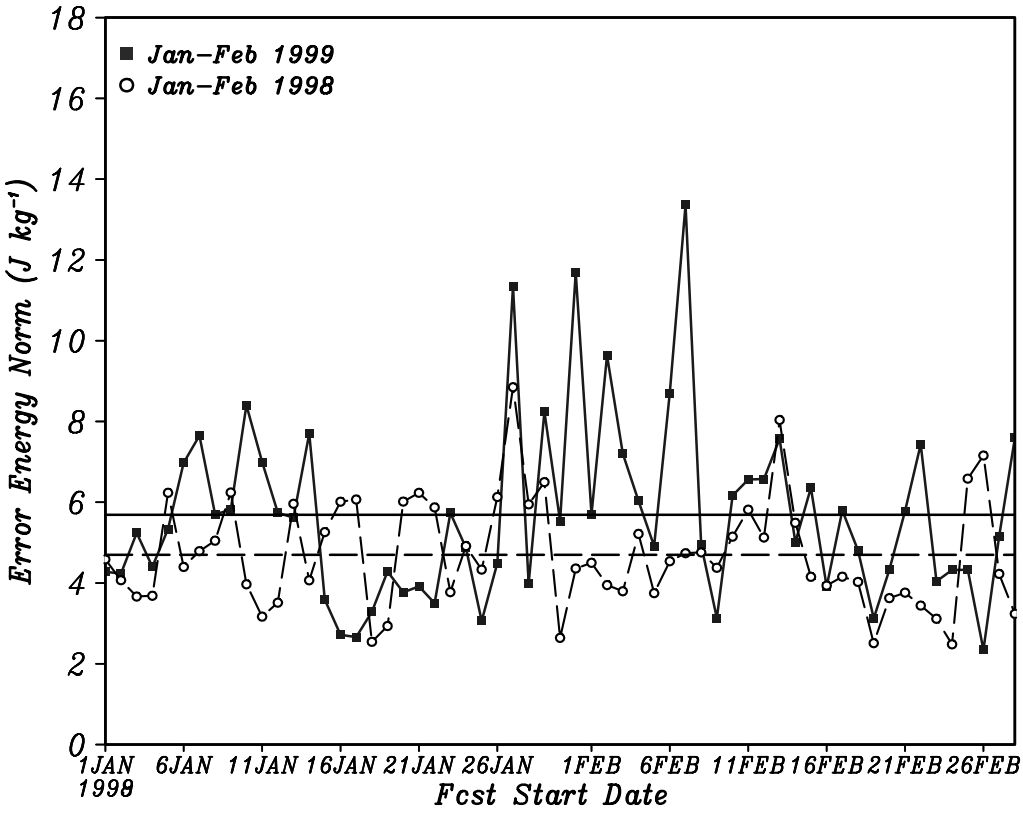

Figure 7. Comparison of 72-hr forecast error over Western North America during January and February 1998 (dash) and 1999 (solid). The error is measured using an energy-weighted sum of temperature, wind and pressure on all model levels from the surface to 150 mb. The verification region is 30°–60°N, 100°–150°W. Forecasts and verifying analyses (incorporating all available observational data) are produced using NOGAPS at T79L18 resolution.